5-2015

Phase Diagrams for Three-Body and Four-Body Systems in One Dimension

Connor D. Morehead
Trinity University, cmorehea@trinity.edu

PHASE DIAGRAMS FOR THREE-BODY AND FOUR-BODY SYSTEMS IN ONE DIMENSION

Connor D. Morehead

A DEPARTMENT HONORS THESIS SUBMITTED TO THE
DEPARTMENT OF PHYSICS AND ASTRONOMY AT TRINITY UNIVERSITY
IN PARTIAL FULFILLMENT OF THE REQUIREMENTS FOR GRADUATION WITH DEPARTMENTAL HONORS

April 16, 2015

_____	_____
Nirav P. Mehta	Dennis Ugolini
THESIS ADVISOR	DEPARTMENT CHAIR

_____
Sheryl Tynes, AVPAA

Student Agreement

I grant Trinity University (“Institution”), my academic department (“Department”), and the Texas Digital Library ("TDL") the non-exclusive rights to copy, display, perform, distribute and publish the content I submit to this repository (hereafter called "Work") and to make the Work available in any format in perpetuity as part of a TDL, Institution or Department repository communication or distribution effort.

I understand that once the Work is submitted, a bibliographic citation to the Work can remain visible in perpetuity, even if the Work is updated or removed.

I understand that the Work's copyright owner(s) will continue to own copyright outside these non-exclusive granted rights.

I warrant that:

1) I am the copyright owner of the Work, or
2) I am one of the copyright owners and have permission from the other owners to submit the Work, or
3) My Institution or Department is the copyright owner and I have permission to submit the Work, or
4) Another party is the copyright owner and I have permission to submit the Work.

Based on this, I further warrant to my knowledge:

1) The Work does not infringe any copyright, patent, or trade secrets of any third party,
2) The Work does not contain any libelous matter, nor invade the privacy of any person or third party, and
3) That no right in the Work has been sold, mortgaged, or otherwise disposed of, and is free from all claims.

I agree to hold TDL, Institution, Department, and their agents harmless for any liability arising from any breach of the above warranties or any claim of intellectual property infringement arising from the exercise of these non-exclusive granted rights.”

I choose the following option for sharing my thesis (required):

[X] Open Access (full-text discoverable via search engines)
[ ] Restricted to campus viewing only (allow access only on the Trinity University campus via digitalcommons.trinity.edu)

I choose to append the following Creative Commons license (optional):

Phase Diagrams for Three-Body and Four-Body Systems in One Dimension

Connor Morehead

April 16, 2015

Contents

1 Abstract **2**

2 Introduction **2**

3 Two-Body Problem **3**

3.1 Delta-Functions 3

3.2 δ-Function Boundary Condition 6

3.3 Bound States 7

3.4 Scattering States and the Effective Range Expansion 7

4 Three-Body Problem **9**

4.1 Coordinates 9

4.2 Born-Oppenheimer Approximation 12

4.3 The 3-Body λ Boundary Condition 13

4.4 Transcendental Equation 14

4.5 3-Body Phase Diagram 15

5 Four-Body Problem **17**

5.1 Coordinates 17

5.2 Born-Oppenheimer Approximation 20

5.3 The 4-Body λ Boundary Condition 21

5.4 4-Body Phase Diagram 23

6 Boundary Conditions with B-Splines **26**

7 Conclusion **27**

8 Acknowledgements **28**

References **28**

1 Abstract

The phase diagrams for three-body and four-body systems with δ-function interactions are presented. The three-body and four body systems considered are the heavy-heavy-light (HHL) and heavy-heavy-heavy-light (HHHL) systems, respectively. The heavy particles are assumed to be identical. Both systems are treated within the Born-Oppenheimer approximation. The results from [16] are extended to arbitrary values of the heavy-heavy (HH) coupling. The phase diagram presented in [8] is reproduced, and the corresponding HHHL phase-diagram is presented. It was found that in both the three and four body systems the scattering lengths (atom-dimer for HHL and atom-trimer for HHHL) and spectra vary smoothly as the heavy-heavy interaction strength λ is varied from 0 to ∞.

2 Introduction

Few-body physics has been an important area of quantum mechanics since its inception. In few-body physics small systems involving 2-6 particles are built up from first principles. Since the Schrödinger equation is a DN-dimensional differential equation, where D is the number of spatial dimensions and N is the number of particles, very few quantum systems can be solved analytically. Thus, physicists have had to resort to increasingly complicated approximations in order to probe such systems. Work in few-body physics has relevance to many other areas of physics such as subnuclear physics, atomic physics, nuclear physics, solid-state physics, and more [20].

There is a large body of literature on few- and many-body physics of strongly interacting 1D systems [13, 14, 24, 23, 4, 21]. These calculations are helpful in building up to full three-dimensional problems, but also are directly related current experiments in quasi-1D cold atomic gases. The Olshanii formula [18, 1] relates the three dimensional scattering length a_{3D} and the transverse oscillator length $a_\perp$ with the one-dimensional scattering length a:

$$a = -\frac{a_\perp^2}{2a_{3D}}\left(1 - C\frac{a_{3D}}{a_\perp}\right) \tag{1}$$

The scattering length, generally speaking, describes the interaction strength between two scattering particles in the limit of zero collision energy. With δ-function interactions, the scattering length is related to the interaction strength of the delta function by:

$$a \propto -\frac{1}{g} \tag{2}$$

From Eq. (2), zero scattering length corresponds to infinitely interacting particles, and infinite scattering length corresponds to zero interaction between particles. The scattering length will be more rigorously defined and discussed in section (3). One can refer to figure (1) for a graphical representation of the scattering length. Current experiments with cold atoms in quasi-1D are able to independently control the three-dimensional scattering length a_{3D} and the transverse oscillator length $a_\perp$. The Olshanii formula allows one to calculate the exact 1D scattering length from other a_{3D} and $a_\perp$. C is a unit-less constant calculated to be ≈ 1.46. In this way the 1D physics is directly related to the 3D physics.

The work of Kartavtsev, et. al. [8] is particularly relevant to this thesis. In reference [8] Kartavtsev, et. al. construct a three-body "HHL" phase diagram which is recreated in this work using different methods. This thesis is based on calculations performed by Mehta [16], and thus one can refer to [16].

Cold atom experiments are now sophisticated enough to directly relate to this thesis. For instance, experiments can create one-dimensional trap geometries and control the interactions between different species of particles [6, 5, 22, 9, 10, 11]. More and more atomic species are able to be trapped, cooled, and studied, giving rise to a diverse set of current experiments. These include experiments being done by the groups of D. Weiss at Pennsylvania State [19] and S. Jochim at Heidelberg [17]. [19] confine ultra-cold rubidium atoms into tubes created by 2D optical latices. [17] manages to cool two ultra-cold fermionic atoms into an isolated double-well potential. They have full control over the quantum state of the system (i.e. interaction strength, tunneling rate between wells, and potential geometry).

This thesis is organized as follows: First is a small look at the two-body problem as a point of reference for the more complicated systems. Following are the 3-body and 4-body systems, in which the coordinate systems, the Born-Oppenheimer approximation, and calculations will be briefly outlined. Then potential curves, spectra, atom-dimer and atom-trimer scattering lengths, and phase diagrams for each system will be presented. Next I will present the three and four body phase diagrams. Finally I will end with my conclusions and outlook.

3 Two-Body Problem

3.1 Delta-Functions

For this thesis, all particle-particle interactions will be modeled with delta functions. The delta function is defined as:

$$\int_{-\epsilon}^{+\epsilon} \delta(x)dx = 1, \qquad \epsilon > 0 \tag{3}$$

One common representation for the delta function is as follows:

$$\delta(x) = \lim_{\epsilon \to 0} \begin{cases} \frac{1}{2\epsilon} & |x| < \epsilon \\ 0 & \text{otherwise} \end{cases} \tag{4}$$

When the de Broglie wavelength λ associated with the relative momentum of the colliding partners is much longer than the range, r_0, of the interaction (i.e. $\lambda \gg r_0$) the details of the short-range interactions are not resolved. Without changing the long-range behavior, delta function potentials can be substituted for the short-range potentials, reproducing the appropriate low-energy physics, specifically the scattering length[1]. This idea is summarized in figures (1), (2), and (3). These figures show the wave-function inside a typical potential well. Figures (1) and (2) show a typical potential with range r_0 for negative and positive scattering length. Figure (3) is the same, but with $a \gg r_0$. In that regime ($r_0 \ll a \ll \lambda$), the long range physics is controlled by the scattering length and one can consider $r_0 \to 0$. A more in depth discussion on the scattering length will follow once it has been mathematically defined.

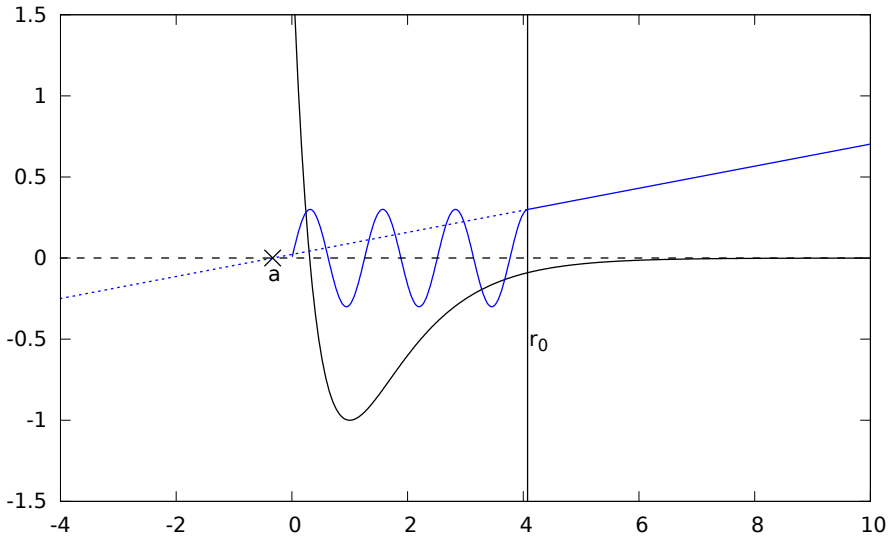

Figure 1: Negative scattering length a in a potential of range r_0.

[1]For a more in depth discussion see ref [12].

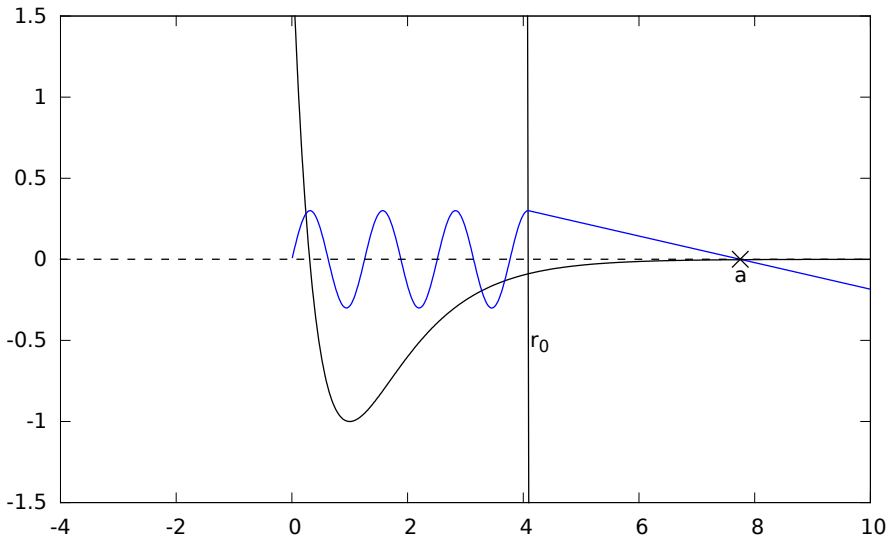

Figure 2: Positive scattering length a in a potential of range r_0.

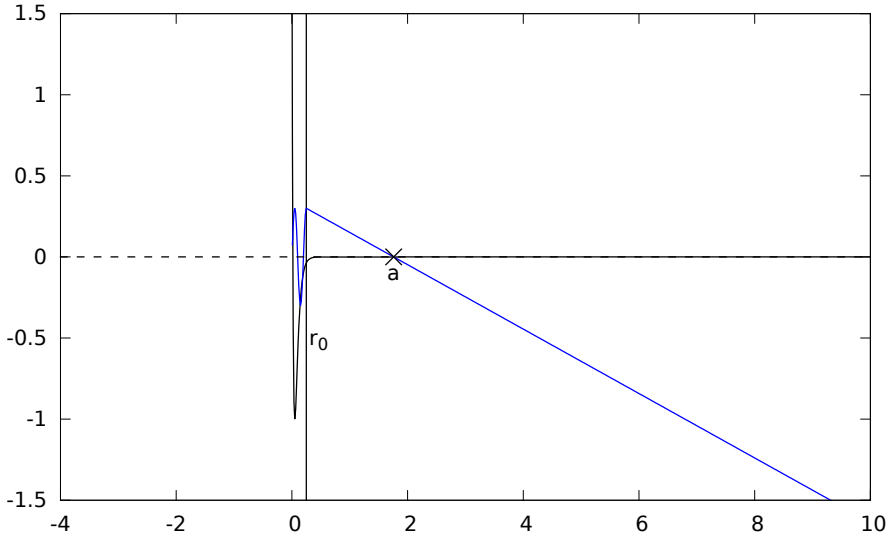

Figure 3: Positive scattering length a in a potential of range r_0.

3.2 δ-Function Boundary Condition

With δ-functions, we can now begin to describe a relevant 2-body problem in one dimension. Let particles 1 and 2 have masses m_1 and m_2. Particles 1 and 2 interact via a δ-function potential given by:

$$V = g\delta(x_1 - x_2) \tag{5}$$

where x_1 and x_2 refer to the positions of particles 1 and 2, respectively and g is the strength of the interaction. The Hamiltonian is thus:

$$H = \frac{p_1^2}{2m_1} + \frac{p_2^2}{2m_2} + V(x_1 - x_2) \tag{6}$$

Rather than dealing with this problem in its full complexity, it is useful to reduce the problem by separating the center of mass motion and the relative particle motion.

$$\begin{aligned} x &= x_1 - x_2 \\ x_{cm} &= \tfrac{m_1 x_1 + m_2 x_2}{m_1 + m_2} \end{aligned} \tag{7}$$

The resulting Hamiltonian is:

$$H = \frac{p_{cm}^2}{2M} + \frac{p_x^2}{2\mu} + V(x) \tag{8}$$

where M is the sum of the masses, μ is the reduced mass, and:

$$\begin{aligned} p_{cm} &= p_1 + p_2 \\ p_x &= \tfrac{m_2 p_1 - m_1 p_2}{m_1 + m_2} \end{aligned} \tag{9}$$

As we can see, the center of mass is separable in this system, meaning we can deal with the inter-particle motion separately from the center of mass motion. The relative Hamiltonian is:

$$H_x = \frac{p_x^2}{2\mu} + V(x) \tag{10}$$

Now all that remains is the familiar delta-function potential problem [7]:

$$-\frac{1}{2\mu}\frac{d^2\psi}{dx^2} + g\delta(x)\psi = E\psi \tag{11}$$

Note that $\hbar$ is set to 1. Multiplying through by -2μ:

$$\frac{d^2\psi}{dx^2} + 2\mu E\psi = 2\mu g\delta(x)\psi \tag{12}$$

by integrating both sides we have:

$$\left(\frac{d\psi}{dx}\right)_{+\epsilon} - \left(\frac{d\psi}{dx}\right)_{-\epsilon} = 2\mu g\psi(0) \tag{13}$$

Knowing that $\left(\frac{d\psi}{dx}\right)_{+\epsilon} = -\left(\frac{d\psi}{dx}\right)_{-\epsilon}$ we're left with:

$$\left(\frac{d\psi}{dx}\right)_{\epsilon} = \mu g\psi(0) \tag{14}$$

This expression gives us the log-derivative boundary condition.

$$\lim_{\epsilon\to 0^+}\left(\frac{\psi'}{\psi}\right)_{\epsilon} = \mu g \tag{15}$$

3.3 Bound States

For $E < 0$ (bound states) we have the usual solutions:

$$\psi(x) = Ae^{-\kappa|x|} \tag{16}$$

From the Schrödinger equation, we define $\kappa = \sqrt{-2\mu E}$. By normalizing Eq. (16) we find $A = \sqrt{\kappa}$. We enforce the boundary condition given in Eq. (15). This gives the following bound state energies:

$$E = -\frac{\mu g^2}{2} \tag{17}$$

and

$$\psi(x) = \sqrt{-\mu g}e^{\mu g|x|} \tag{18}$$

3.4 Scattering States and the Effective Range Expansion

When $E > 0$ we instead have scattering solutions. Begin by noting that for $V(x) = 0$, the positive-parity free-particle solution is given by:

$$\psi(x) = \cos(kx) \tag{19}$$

where $k = \sqrt{2\mu E}$. When $V(x) \neq 0$ but $V(x) = 0$ for some $x > x_0$ we have:

$$\psi(x) \to \cos(kx + \delta), \quad \forall \ \ x > x_0 \tag{20}$$

where δ is the phase shift. Note we can ignore the overall normalization since these states are not normalizable at all. We can then expand this solution using a trigonometric identity for cosine:

$$\psi(x) \to \cos(kx)\cos(\delta) - \sin(kx)\sin(\delta), \quad \forall \ \ x > x_0 \tag{21}$$

Again, ignoring overall normalization,

$$\psi(x) \to \cos(kx) - \tan(\delta)\sin(kx), \quad \forall \ \ x > x_0 \tag{22}$$

We now substitute Eq. (22) into Eq. (15):

$$\left.\frac{\psi'}{\psi}\right|_{x_0} = \left.\frac{-k\sin(kx) - k\tan(\delta)\cos(kx)}{\cos(kx) - \tan(\delta)\sin(kx)}\right|_{x_0} \tag{23}$$

Typically the log-derivative on the left hand side is obtained from the numerical solutions to the Schrödinger equation for $x \leq x_0$. Upon solving the above equation for $k\tan(\delta)$ and taking the limit $k \to 0$, one obtains the one-dimensional scattering length:

$$\lim_{k\to 0} k\tan(\delta) = \frac{1}{a} \tag{24}$$

Specifically for a δ-function interaction of the form of Eq. (5), one obtains:

$$a = -\frac{1}{\mu g} \tag{25}$$

Note the scattering length depends on the interaction between the scattering particles. In this way, the scattering length can be thought of as a way of describing the particle-particle interactions. In the lab, this 1D scattering length is controlled by a_{3D} and $a_\perp$ from Eq. (1).

The other important way to think about the scattering length is encapsulated in figures (1), (2), and (3). In these figures we have the long range solutions (the straight lines) which intersect with the x-axis for positive scattering length. For negative scattering length, one simply traces the long range solution back down to the x-intercept. This can be seen mathematically by taking Eq. (22) and taking the limit as $k \to 0$.

$$\lim_{k\to 0} \cos(kx) - \tan(\delta)\sin(kx) = 1 - k\tan(\delta)x \tag{26}$$

One then simply sets Eq. (26) to 0 and solves for x to find the x-intercept. It's a simple matter to confirm the same result as in Eq. (24).

When considering the scattering length from this perspective, one can use the scattering length to obtain useful information about the number of bound states. As the wave-function shown in figures (1) and (2) accumulates phase, the scatting length becomes more and more negative. Eventually, the wave-function will acquire another node and the scattering length will become positive. The new node shows the presence of a new bound state supported by the potential. Thus when the scattering length changes from $-\infty$ to ∞, we expect a new bound state to appear.

4 Three-Body Problem

4.1 Coordinates

Suppose we have three particles in one dimension. Let particles 1 and 2 have mass $m_1 = m_2 = m_H$ and particle 3 has mass $m_L = \beta m_H$. Thus we have the mass ratio:

$$\beta \equiv \frac{m_L}{m_H} \tag{27}$$

β is one of the main parameters in this work, as it is controllable in the lab through the choice of cooled atoms. We assume δ-function heavy-light interactions given by:

$$V_{ij} = g\delta(x_i - x_j) \tag{28}$$

From Eq. (24) the one-dimensional H-L scattering length is given by $a = -1/(\mu_{HL} g)$. By assuming $a > 0$ the heavy-light binding energy is $B_2 = \mu_{HL} g^2/2 = 1/(2\mu_{HL} a^2)$. The positions of particles 1, 2, and 3, are given by x_1, x_2, and x_3, respectively. We have the Hamiltonian:

$$H = \sum_i -\frac{1}{2m_i}\frac{\partial^2}{\partial x_i^2} + \sum_{ij} V_{ij} \tag{29}$$

We introduce the following change of coordinates:

$$y_1 = \sqrt{\frac{\mu_{12}}{\mu_{3b}}}(x_2 - x_1) \tag{30}$$

$$y_2 = \sqrt{\frac{\mu_{12,3}}{\mu_{3b}}}\left(\frac{m_1 x_1 + m_2 x_2}{m_1 + m_2} - x_3\right) \tag{31}$$

$$y_3 = \sqrt{\frac{1}{\mu_{3b}}}\left(\frac{m_1 x_1 + m_2 x_2 + m_3 x_3}{m_1 + m_2 + m_3}\right) \tag{32}$$

The reduced masses are:

$$\mu_{12} = m_H/2 \tag{33}$$

$$\mu_{12,3} = m_H[2\beta/(2+\beta)] \tag{34}$$

$$\mu_{3b} = \sqrt{\mu_{12}\mu_{12,3}} \tag{35}$$

$$\mu_{HL} = m_H[\beta/(1+\beta)] \tag{36}$$

The Hamiltonian then becomes:

$$H = -\frac{1}{2\mu_{3b}}\left(\frac{\partial^2}{\partial y_1^2} + \frac{\partial^2}{\partial y_2^2} + \frac{\partial^2}{\partial y_3^2}\right) + g_{HH}\delta\left(\left(\frac{\beta}{2+\beta}\right)^{1/4}\sqrt{2}y_1\right) + g_{HL}\delta\left(\frac{\sqrt{\beta(2+\beta)}y_1 - (2+\beta)y_2}{\sqrt{2}(2+\beta)^{3/4}\beta^{1/4}}\right) + g_{HL}\delta\left(\frac{\sqrt{\beta(2+\beta)}y_1 + (2+\beta)y_2}{\sqrt{2}(2+\beta)^{3/4}\beta^{1/4}}\right) \tag{37}$$

At this point we ignore the center of mass motion and only consider the relative motion. The Hamiltonian is then:

$$H = -\frac{1}{2\mu_{3b}}\left(\frac{\partial^2}{\partial y_1^2} + \frac{\partial^2}{\partial y_2^2}\right) + g_{HH}\delta\left(\left(\frac{\beta}{2+\beta}\right)^{1/4}\sqrt{2}y_1\right) + g_{HL}\delta\left(\frac{\sqrt{\beta(2+\beta)}y_1 - (2+\beta)y_2}{\sqrt{2}(2+\beta)^{3/4}\beta^{1/4}}\right) + g_{HL}\delta\left(\frac{\sqrt{\beta(2+\beta)}y_1 + (2+\beta)y_2}{\sqrt{2}(2+\beta)^{3/4}\beta^{1/4}}\right) \tag{38}$$

After some careful algebra and repeated use of:

$$\delta(f(x)) = \frac{\delta(x - x_0)}{\left|\frac{\partial f}{\partial x}\right|_{x_0}} \tag{39}$$

where x_0 is the zero of $f(x)$, we have:

$$H = -\frac{1}{2\mu_{3b}}\left(\frac{\partial^2}{\partial y_1^2}+\frac{\partial^2}{\partial y_2^2}\right) - \sqrt{2}\left(\frac{\beta}{2+\beta}\right)^{1/4}\left[g_{HH}\delta\left(2\sqrt{\frac{\beta}{2+\beta}}y_1\right)\right.$$
$$\left. + g_{HL}\delta\left(y_2-\sqrt{\frac{\beta}{2+\beta}}y_1\right) + g_{HL}\delta\left(y_2+\sqrt{\frac{\beta}{2+\beta}}y_1\right)\right] \quad (40)$$

The Hamiltonian is then scaled by the heavy-light binding energy given by:

$$B_2 = \frac{1}{m_H a^2}\frac{\beta+1}{2\beta} \quad (41)$$

This is accomplished by simply dividing the entire Schrödinger equation by the heavy-light binding energy. We define our energy scale in terms of B_2 simply to have an explicit energy scale. The Hamiltonian reads:

$$H = -\frac{1}{2\frac{1+\beta}{2\sqrt{\beta(2+\beta)}}}\left(\frac{\partial^2}{\partial\left(\frac{y_1}{a}\right)^2}+\frac{\partial^2}{\partial\left(\frac{y_2}{a}\right)^2}\right) - 2\sqrt{2}\left(\frac{\beta}{2+\beta}\right)^{1/4}\left[\frac{g_{HH}}{g_{HL}}\delta\left(2\sqrt{\frac{\beta}{2+\beta}}\frac{y_1}{a}\right)\right.$$
$$\left. + \delta\left(\frac{y_2}{a}-\sqrt{\frac{\beta}{2+\beta}}\frac{y_1}{a}\right) + \delta\left(\frac{y_2}{a}+\sqrt{\frac{\beta}{2+\beta}}\frac{y_1}{a}\right)\right] \quad (42)$$

We introduce the following unit-less mass-scaled Jacobi coordinates and the following parameters:

$$x = \frac{1}{a}y_1 \quad (43)$$
$$y = \frac{1}{a}y_2 \quad (44)$$
$$\mu_3 = \frac{1+\beta}{2\sqrt{\beta(2+\beta)}} \quad (45)$$
$$g_3 = -2\sqrt{2}\left(\frac{\beta}{2+\beta}\right)^{1/4} \quad (46)$$
$$\lambda = \frac{g_{HH}}{g_{HL}} \quad (47)$$
$$x_0 = x\sqrt{\frac{\beta}{2+\beta}} \quad (48)$$

thus the Hamiltonian is:

$$H = -\frac{1}{2\mu_3}\left(\frac{\partial^2}{\partial x^2}+\frac{\partial^2}{\partial y^2}\right) + g_3[\lambda\delta(2x_0)+\delta(y+x_0)+\delta(y-x_0)] \quad (49)$$

Finally, the Schrödinger equation reads:

$$-\frac{1}{2\mu_3}\left(\frac{\partial^2}{\partial x^2}+\frac{\partial^2}{\partial y^2}\right)\Psi(x,y)+g_3[\lambda\delta(2x_0)+\delta(y+x_0)+\delta(y-x_0)]\Psi(x,y)=E\Psi(x,y) \tag{50}$$

λ, the ratio of heavy-heavy to heavy-light couplings is of particular importance to this work. In [16], only $\lambda = 0$ and $\lambda = \infty$ are considered. This thesis extends the results of [16] to arbitrary λ.

4.2 Born-Oppenheimer Approximation

We invoke the Born-Oppenheimer approximation:

$$\Psi(x,y)=\Phi(x;y)\psi(x) \tag{51}$$

In short, the Born-Oppenheimer approximation asserts that the heavy particles are essentially at rest when compared to the light particle, fixing the x-coordinate. This allows us to separate Ψ into the product seen in Eq. (51) where $\Phi(x;y)$ depends adiabatically on x and $\psi(x)$ depends only on x. For a more complete description, see [3]. The wave-function $\Phi(x;y)$ satisfies the following fixed-x equation.

$$\left[\frac{-1}{2\mu_3}\frac{\partial^2}{\partial y^2}+g_3[\delta(y+x_0)+\delta(y-x_0)]\right]\Phi(x;y)=u(x)\Phi(x;y) \tag{52}$$

$u(x) < 0$ is the Born-Oppenheimer potential in units of the H-L binding energy. To solve this equation, one fixes x and integrates over the remaining y coordinate. This is shown visually in figure (4). Inserting Eq. (51) into Eq.(50) and using Eq. (52) we have:

$$\left(\frac{-1}{2\mu_3}\frac{\partial^2}{\partial x^2}+g_3\lambda\delta(2x_0)+u(x)+\frac{\widetilde{Q}(x)}{2\mu_3}\right)\psi(x)=E\psi(x) \tag{53}$$

where

$$\widetilde{Q}(x)=\left\langle\frac{\partial\Phi}{\partial x}\,\middle|\,\frac{\partial\Phi}{\partial x}\right\rangle_y \tag{54}$$

The integration of the matrix element $\widetilde{Q}(x)$ is carried out over the y coordinate while the adiabatic coordinate x is held fixed.

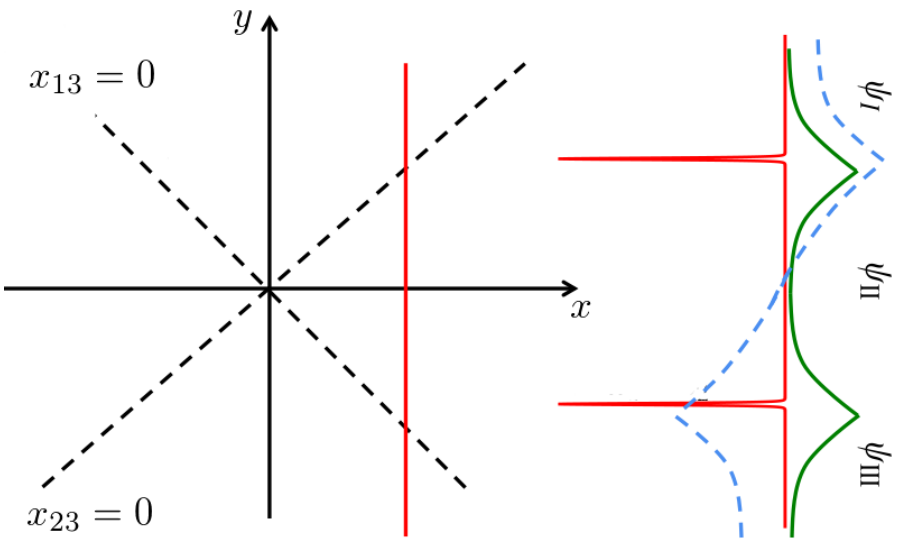

Figure 4: On the left is the x-y plane which shows the HL coalescence points as the dotted lines. On the right is the resultant 1D double-δ-function problem which is solved over y. Figures adapted from [15] with permission.

$\lambda = 0$ (Non-Interacting Bosons)	$\lambda = \infty$ (Infinitely Repulsive Bosons)
$\psi'\|_{x=0} = 0$	$\psi\|_{x=0} = 0$

Table 1: Previous boundary conditions on ψ in [16]

4.3 The 3-Body λ Boundary Condition

In Ref. [16] only $\lambda \to 0$ and $\lambda \to \infty$ were considered. For these cases, the boundary conditions on $\psi(x)$ at $x = 0$ are shown in Table (1). Here, we derive a new boundary condition for arbitrary λ at $x = 0$. Notice Eq. (53) is similar in form to Eq. (11). In order to derive a new boundary condition for Eq. (53), we use the same method used to derive the boundary condition for Eq. (11). Rearranging Eq. (53) we have:

$$\frac{\partial^2 \psi}{\partial x^2} = 2\mu_3 g_3 \lambda \delta(x_0)\psi + [\widetilde{Q}(x) + 2\mu_3 u(x) - 2\mu_3 E)]\psi \tag{55}$$

Integrating both sides across an interval 2ϵ about 0 and implicitly considering the limit $\epsilon \to 0$ we have:

$$\left.\frac{d\psi}{dx}\right|_{+\epsilon} - \left.\frac{d\psi}{dx}\right|_{-\epsilon} = \sqrt{\frac{2+\beta}{\beta}}\mu_3 g_3 \lambda \psi(0) + \int_{-\epsilon}^{+\epsilon} (\widetilde{Q}(x) + 2\mu_3 u(x) - 2\mu_3 E)\psi \tag{56}$$

Utilizing the fact that $\left.\frac{d\psi}{dx}\right|_{-\epsilon} = -\left.\frac{d\psi}{dx}\right|_{+\epsilon}$ we have:

$$\left.\frac{d\psi}{dx}\right|_{+\epsilon} = \sqrt{\frac{2+\beta}{\beta}}\frac{\mu_3 g_3 \lambda}{2}\psi(0) + \frac{1}{2}\int_{-\epsilon}^{+\epsilon} (\widetilde{Q}(x) + 2\mu_3 u(x) - 2\mu_3 E)\psi \tag{57}$$

We then take the limit as $\epsilon \to 0$ and are left with:

$$\left.\frac{\psi'}{\psi}\right|_{\epsilon\to 0} = \sqrt{\frac{2+\beta}{\beta}}\frac{\mu_3 g_3 \lambda}{2} + \frac{1}{2}\int_{-\epsilon}^{+\epsilon}(\widetilde{Q}(x) + 2\mu_3 u(x) - 2\mu_3 E)\psi \to 0 \tag{58}$$

Plugging in expressions for μ_3 and g_3 we're left with the following boundary condition:

$$\left.\frac{\psi'}{\psi}\right|_{\epsilon\to 0} = -\frac{1+\beta}{\sqrt{2\beta}\sqrt[4]{\beta(2+\beta)}}\lambda \tag{59}$$

This boundary condition is shown being enforced for different values of λ in figure 5.

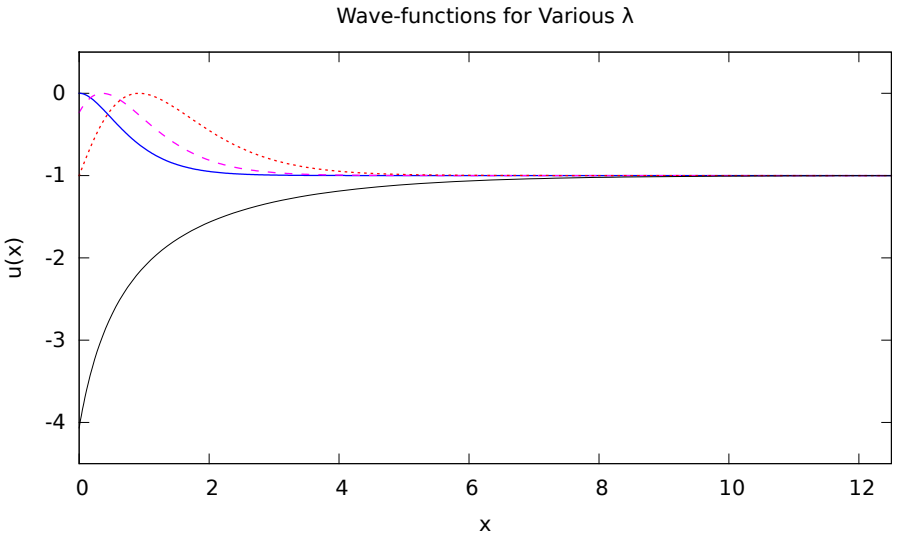

Figure 5: $\psi(x)$, the solution to Eq. (52), is shown for three values of λ. $\lambda = 0$ is the blue solid curve, $\lambda = 0.3$ is the purple dashed curve, and $\lambda = \infty$ is the red dotted line. The solid black line is the 3-body potential curve. All ψs and potentials are calculated for $\beta = 22.08$, the mass ratio for Cs-Li mixtures.

4.4 Transcendental Equation

The solutions to Eq. (52) are:

$$\Phi(x;y) = \begin{cases} A\sinh(\kappa y) + B\cosh(\kappa y), & \text{if} \quad 0 \le y \le x_0 \\ De^{-\kappa y}, & \text{if} \quad x_0 \le y \end{cases} \tag{60}$$

where $\kappa = \sqrt{-2\mu_3 u(x)}$. By then matching these two wave-functions and imposing the derivative discontinuity across the δ function at $y = x_0$, we have the following transcendental equation for the eigenvalue

κ:

$$\frac{\kappa}{g_3\mu_3} + 1 = (-1)^{P+1} e^{-2\kappa x_0} \tag{61}$$

Here $P = 0$ corresponds to the even solution ($\frac{\partial \Phi}{\partial y}|_{y=0} = 0$), and $P = 1$ corresponds to the odd solution ($\Phi|_{y=0} = 0$). The solutions to Eq. (61) give potential curves for the HHL system shown in figs. (9)(b), (d), and (f).

4.5 3-Body Phase Diagram

For the scattering solutions of the HHL system the solution to Eq. (53) in the region $x >> l_o$ (l_o is the range of $U(x)$) is matched to

$$\psi(x) \to \begin{cases} \cos(kx) - \tan(\delta)\sin(kx) & \text{bosons}, \quad x > 0 \\ \sin(kx) + \tan(\delta)\cos(kx) & \text{fermions}, \quad x > 0 \end{cases} \tag{62}$$

Note the difference in solutions for bosons and fermions stems simply from their even and odd nature, respectively. These solutions are analogous to the solution from Eq. (22). Thus the atom-dimer scattering length is

$$\frac{1}{a_{AD}} = \lim_{k_{AD}\to 0} \begin{cases} k_{AD}\tan(\delta) & \text{bosons} \\ -k_{AD}\cot(\delta) & \text{fermions} \end{cases} \tag{63}$$

where $k_{AD} = \sqrt{2\mu_{23,1}E_{rel}}$ and $k = \sqrt{\mu_3 E_{rel}}$.

Figure (6)(a) shows the three-body spectrum as a function of $\beta^{-1/2}$. Figure (6)(b) shows the atom-dimer scattering length as a function of $\beta^{-1/2}$. The asymptotes and zeros shown in Figure (6)(b) are calculated via a bisection root-finding algorithm. As the calculation repeats over different values of λ, these asymptotes and zeros are stored and plotted. Figure (7) agrees with the calculations of Ref. [8]. Note our figure does not extend beyond the dotted black line. This line denotes where the HH and HL two-body energies are equal. Our calculation does not consider this area of phase-space, as we have restricted calculation to portions of the phase space where the lowest atom-dimer threshold corresponds to the atom-dimer collision $HL + H \to HL + H$. For regions below the dotted black line the lowest two body channel corresponds to the atom-dimer collision $HH + L \to HH + L$, which we do not consider. This phase diagram shows the number of three-body bound states for a given mass ratio and interaction strength, both tunable variables in the lab.

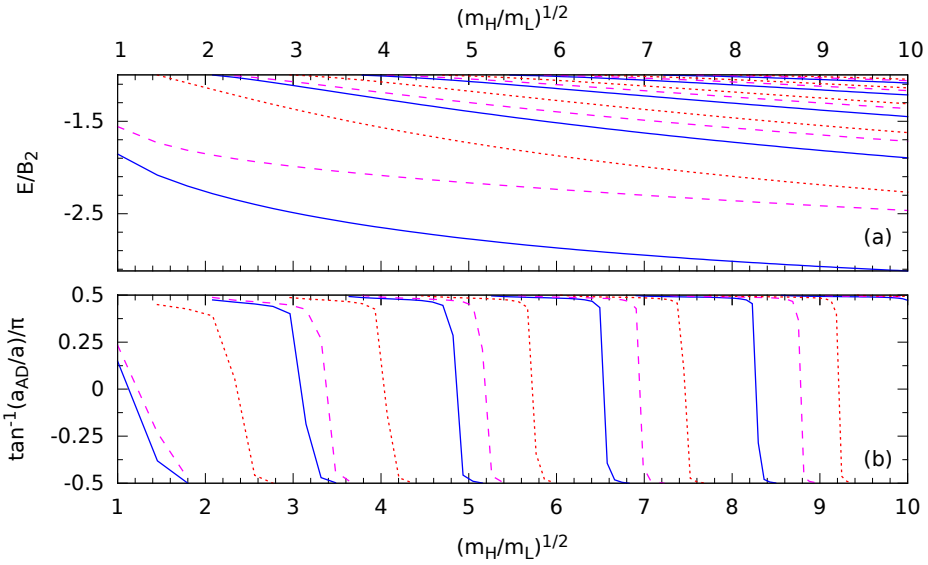

Figure 6: Graph (a) shows the energy spectrum for the three-body system as a function of $\beta^{-1/2}$. Graph (b) shows $\tan^{-1}(a_{AD}/a)/\pi$, where a_{AD} is the atom-dimer scattering length. Solid blue curves represent the noninteracting bosonic H particles ($\lambda = 0$). The dashed purple curves represent the interacting bosonic H particles ($\lambda = 0.3$). The dotted red curves represent the noninteracting fermionic particles or fermionized H particles with $\lambda = \infty$.

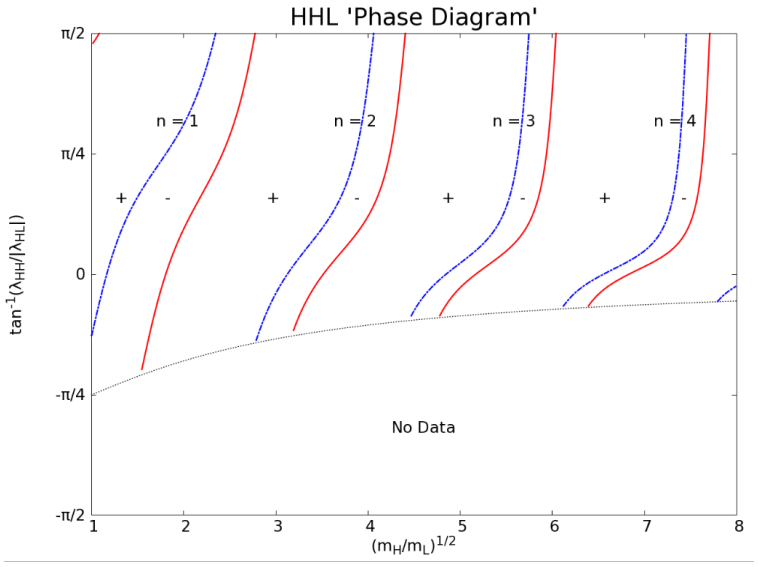

Figure 7: Phase diagram for the HHL system as a function of $\beta^{-1/2}$ and $\arctan(\lambda)$. The dash-dotted blue line denotes the positions of the zeros (i.e. where the atom-dimer scattering length changes sign). The solid red curves denote the positions of the asymptotes (i.e. where the system begins to support a new bound-state). The dotted black line represents where the HH and HL two-body energies are equal. The number of three-body bound states is indicated by n on the graph.

5 Four-Body Problem

5.1 Coordinates

The four-body problem is set up in a similar manner to the three-body problem. Particles 1, 2, and 3 have masses $m_1 = m_2 = m_3 = m_H$ and particle 4 has mass $m_4 = m_L = \beta m_H$. The scaling of the Schrödinger equation follows as it did in the HHL problem. We begin with the familiar Hamiltonian:

$$H = \sum_i -\frac{1}{2m_i}\frac{\partial^2}{\partial x_i^2} + \sum_{ij} V_{ij} \tag{64}$$

We introduce the following change of coordinates:

$$y_1 = \sqrt{\frac{\mu_{12}}{\mu_{4b}}}(x_1 - x_2) \tag{65}$$

$$y_2 = \sqrt{\frac{\mu_{12,3}}{\mu_{4b}}}\left(\frac{m_1x_1 + m_2x_2}{m_1 + m_2} - x_3\right) \tag{66}$$

$$y_3 = \sqrt{\frac{\mu_{123,4}}{\mu_{4b}}}\left(\frac{m_1x_1 + m_2x_2 + m_3x_3}{m_1 + m_2 + m_3} - x_4\right) \tag{67}$$

$$y_4 = \sqrt{\frac{1}{\mu_{4b}}}\left(\frac{m_1x_1 + m_2x_2 + m_3x_3 + m_4x_4}{m_1 + m_2 + m_3 + m_4}\right) \tag{68}$$

Ignoring the center of mass motion, the Hamiltonian is thus:

$$\begin{aligned} H = &-\frac{1}{2\mu_{4b}}\left(\frac{\partial^2}{\partial y_1^2} + \frac{\partial^2}{\partial y_2^2} + \frac{\partial^2}{\partial y_3^2}\right) + \\ &g_{HH}\left(\delta\left(\left(\frac{\beta}{3+\beta}\right)^{1/6}\sqrt{2}y_1\right) + \delta\left(\frac{1}{\sqrt{2}}\left(\frac{\beta}{3+\beta}\right)^{1/6}(y_1 + \sqrt{3}y_2)\right) + \right. \\ &\left.\delta\left(\frac{1}{\sqrt{2}}\left(\frac{\beta}{3+\beta}\right)^{1/6}(-y_1 + \sqrt{3}y_2)\right)\right) + \\ &g_{HL}\left(\delta\left(\frac{1}{6}\frac{3\sqrt{2\beta(3+\beta)}y_1 + \sqrt{6\beta(3+\beta)}y_2 + 2\sqrt{3}(3+\beta)y_3}{(3+\beta)^{2/3}\beta^{1/3}}\right) + \right. \\ &\left.\delta\left(\frac{1}{6}\frac{-3\sqrt{2\beta(3+\beta)}y_1 + \sqrt{6\beta(3+\beta)}y_2 + 2\sqrt{3}(3+\beta)y_3}{(3+\beta)^{2/3}\beta^{1/3}}\right) + \delta\left(-\frac{1}{\sqrt{3}}\frac{\sqrt{2\beta(3+\beta)}y_2 - (3+\beta)y_3}{(3+\beta)^{2/3}\beta^{1/3}}\right)\right) \end{aligned} \tag{69}$$

First we will consider the heavy-heavy interactions separately.

$$\begin{aligned} V_{12} + V_{13} + V_{23} = g_{HH}&\left(\delta\left(\left(\frac{\beta}{3+\beta}\right)^{1/6}\sqrt{2}y_1\right) + \delta\left(\frac{1}{\sqrt{2}}\left(\frac{\beta}{3+\beta}\right)^{1/6}(y_1 + \sqrt{3}y_2)\right) + \right. \\ &\left.\delta\left(\frac{1}{\sqrt{2}}\left(\frac{\beta}{3+\beta}\right)^{1/6}(-y_1 + \sqrt{3}y_2)\right)\right) \end{aligned} \tag{70}$$

After some simplification we have:

$$V_{12}+V_{13}+V_{23}=\frac{g_{HH}}{\sqrt{2}}\left(\frac{3+\beta}{\beta}\right)^{1/6}\left(\delta(y_1)+\delta\left(\frac{1}{2}y_1+\frac{\sqrt{3}}{2}y_2\right)+\delta\left(\frac{1}{2}y_1-\frac{\sqrt{3}}{2}y_2\right)\right) \tag{71}$$

We then scale by the heavy-light binding energy B_2.

$$\frac{V_{12}+V_{13}+V_{23}}{B_2}=-\sqrt{2}\left(\frac{3+\beta}{\beta}\right)^{1/6}\lambda\left(\delta\left(\frac{y_1}{a}\right)+\delta\left(\frac{1}{2}\frac{y_1}{a}+\frac{\sqrt{3}}{2}\frac{y_2}{a}\right)+\delta\left(\frac{1}{2}\frac{y_1}{a}-\frac{\sqrt{3}}{2}\frac{y_2}{a}\right)\right) \tag{72}$$

We then move to the following unit-less mass-scaled Jacobi coordinates:

$$x=\frac{1}{a}y_1 \tag{73}$$

$$y=\frac{1}{a}y_2 \tag{74}$$

$$z=\frac{1}{a}y_3 \tag{75}$$

where $\mu_{4b}=(\mu_{12}\mu_{12,3}\mu_{123,4})^{1/3}$ is the four-body reduced mass. Thus our scaled heavy-heavy interaction is:

$$\frac{V_{12}+V_{13}+V_{23}}{B_2}=-\sqrt{2}\left(\frac{3+\beta}{\beta}\right)^{1/6}\lambda\left(\delta\left(x\right)+\delta\left(\frac{1}{2}x+\frac{\sqrt{3}}{2}y\right)+\delta\left(\frac{1}{2}x-\frac{\sqrt{3}}{2}y\right)\right) \tag{76}$$

Next we move to hyperspherical coordinates. This is equivalent to moving to spherical-polar coordinates from Cartesian coordinates.

$$x=\rho\cos(\phi) \tag{77}$$

$$y=\rho\sin(\phi) \tag{78}$$

$$z=R\cos(\theta) \tag{79}$$

$$\rho=\sqrt{x^2+y^2} \tag{80}$$

$$\rho=R\sin(\theta) \tag{81}$$

We can now re-write the heavy-heavy interaction as:

$$\frac{V_{12}+V_{13}+V_{23}}{B_2}=-\sqrt{2}\left(\frac{3+\beta}{\beta}\right)^{1/6}\lambda\left[\delta(\rho\cos(\phi))+\delta(\rho\cos(\phi-\pi/3))+\delta(-\rho\cos(\phi+\pi/3))\right] \tag{82}$$

We then rearrange and have:

$$\frac{V_{12}+V_{13}+V_{23}}{B_2} = \lambda g_4 \sum_{i<j}^{3} \delta(\alpha\rho|\sin(\phi-\phi_{ij})|) \tag{83}$$

with:

$$\alpha = \sqrt{\frac{6\beta}{3+\beta}} \tag{84}$$

$$\phi_{12} = \frac{\pi}{2} \tag{85}$$

$$\phi_{23} = -\phi_{13} = \frac{\pi}{6} \tag{86}$$

$$g_4 = -2\sqrt{3}\left(\frac{\beta}{3+\beta}\right)^{1/3} \tag{87}$$

Note that this formula for α is a correction to [16]. Returning our attention to the rest of the Hamiltonian we're left with:

$$-\frac{1}{2\mu_{4b}}\left(\frac{\partial^2}{\partial y_1^2}+\frac{\partial^2}{\partial y_2^2}+\frac{\partial^2}{\partial y_3^2}\right)+g_{HL}\left(\delta\left(\frac{1}{6}\frac{3\sqrt{2\beta(3+\beta)}y_1+\sqrt{6\beta(3+\beta)}y_2+2\sqrt{3}(3+\beta)y_3}{(3+\beta)^{2/3}\beta^{1/3}}\right)+\right.$$
$$\left.\delta\left(\frac{1}{6}\frac{-3\sqrt{2\beta(3+\beta)}y_1+\sqrt{6\beta(3+\beta)}y_2+2\sqrt{3}(3+\beta)y_3}{(3+\beta)^{2/3}\beta^{1/3}}\right)+\delta\left(-\frac{1}{\sqrt{3}}\frac{\sqrt{2\beta(3+\beta)}y_2-(3+\beta)y_3}{(3+\beta)^{2/3}\beta^{1/3}}\right)\right) \tag{88}$$

After some simplifications we end up with:

$$-\frac{1}{2\mu_{4b}}\left(\frac{\partial^2}{\partial y_1^2}+\frac{\partial^2}{\partial y_2^2}+\frac{\partial^2}{\partial y_3^2}\right)+g_{HL}\sqrt{3}\left(\frac{\beta}{3+\beta}\right)^{1/3}\left(\delta\left(y_3+\sqrt{\frac{\beta}{2(3+\beta)}}(\sqrt{3}y_1+y_2)\right)+\right.$$
$$\left.\delta\left(y_3+\sqrt{\frac{\beta}{2(3+\beta)}}(-\sqrt{3}y_1+y_2)\right)+\delta\left(y_3-\sqrt{\frac{2\beta}{3+\beta}}y_2\right)\right) \tag{89}$$

We then scale the Hamiltonian with the heavy-light binding energy B_2:

$$-\frac{1}{2}\frac{2\beta^{2/3}(3+\beta)^{1/3}}{\beta+1}\left(\frac{\partial^2}{\partial\left(\frac{y_1}{a}\right)}+\frac{\partial^2}{\partial\left(\frac{y_2}{a}\right)}+\frac{\partial^2}{\partial\left(\frac{y_3}{a}\right)}\right)-2\sqrt{3}\left(\frac{\beta}{3+\beta}\right)^{1/3}$$
$$\left(\delta\left(\frac{y_3}{a}+\sqrt{\frac{\beta}{2(3+\beta)}}\left(\sqrt{3}\frac{y_1}{a}+\frac{y_2}{a}\right)\right)+\delta\left(\frac{y_3}{a}+\sqrt{\frac{\beta}{2(3+\beta)}}\left(-\sqrt{3}\frac{y_1}{a}+\frac{y_2}{a}\right)\right)+\right.$$
$$\left.\delta\left(\frac{y_3}{a}-\sqrt{\frac{2\beta}{3+\beta}}\frac{y_2}{a}\right)\right) \tag{90}$$

We then move to the Jacobi coordinates from Eqs. (73), (74), and (75).

$$-\frac{1}{2\mu_4}\left(\frac{\partial^2}{\partial x^2}+\frac{\partial^2}{\partial y^2}+\frac{\partial^2}{\partial z^2}\right)+g_4\left(\delta\left(z+\sqrt{\frac{\beta}{2(3+\beta)}}\left(\sqrt{3}x+y\right)\right)+\right.$$
$$\left.\delta\left(z+\sqrt{\frac{\beta}{2(3+\beta)}}\left(-\sqrt{3}x+y\right)\right)+\delta\left(z-\sqrt{\frac{2\beta}{3+\beta}}y\right)\right) \quad (91)$$

with:

$$\mu_4=\frac{\beta+1}{2\beta^{2/3}(3+\beta)^{1/3}} \quad (92)$$

Next we move to x and y to the hyperspherical coordinates in Eqs. (77), (78), (79), (80), and (81).

$$-\frac{1}{2\mu_4}\left(\frac{1}{\rho}\frac{\partial}{\partial\rho}\rho\frac{\partial}{\partial\rho}+\frac{1}{\rho^2}\frac{\partial^2}{\partial\phi^2}+\frac{\partial^2}{\partial z^2}\right)+g_4\left(\delta\left(z+\sqrt{\frac{2\beta}{3+\beta}}\rho\left(\frac{\sqrt{3}}{2}\cos(\phi)+\frac{1}{2}\sin(\phi)\right)\right)+\right.$$
$$\left.\delta\left(z+\sqrt{\frac{2\beta}{3+\beta}}\rho\left(\frac{-\sqrt{3}}{2}\cos(\phi)+\frac{1}{2}\sin(\phi)\right)\right)+\delta\left(z-\sqrt{\frac{2\beta}{3+\beta}}\rho\sin(\phi)\right)\right) \quad (93)$$

Utilizing trigonometric substitutions, the Hamiltonian becomes:

$$-\frac{1}{2\mu_4}\nabla^2+g_4\sum_{i=1}^{3}\delta(z-z_i) \quad (94)$$

with:

$$z_i=\sqrt{\frac{2\beta}{3+\beta}}\rho\sin\left(\phi-\phi_i\right) \quad (95)$$

where $\phi_1=-4\pi/3$, $\phi_2=0$, and $\phi_3=-2\pi/3$. We rescaled the Schrödinger equation by the heavy-light binding energy B_2. Finally the full four-body Schrödinger equation reads:

$$-\frac{1}{2\mu_4}\nabla^2\Psi(\rho,\phi,z)+\left[g_4\sum_{i=1}^{3}\delta(z-z_i)+\lambda g_4\sum_{i<j}^{3}\delta(\alpha\rho|\sin\phi-\phi_{ij}|)\right]\Psi(\rho,\phi,z)=E\Psi(\rho,\phi,z) \quad (96)$$

5.2 Born-Oppenheimer Approximation

By fixing x and y, one equivalently fixes ρ, and ϕ. We make the Born-Oppenheimer factorization:

$$\Psi=\Phi(\rho,\phi;z)\psi(\rho,\phi) \quad (97)$$

where the adiabatic equation for the Born-Oppenheimer surface is:

$$\left(-\frac{1}{2\mu_4}\frac{\partial^2}{\partial z^2}+g_4\sum_{i=1}^{3}\delta(z-z_i)\right)\Phi(\rho,\phi;z)=U(\rho,\phi)\Phi(\rho,\phi;z) \tag{98}$$

The heavy-particle eigenstates now live on the potential-energy surface $U(\rho,\phi)$, and satisfy (in the extreme adiabatic approximation (EAA)):

$$-\frac{1}{2\mu_4}\left(\frac{1}{\rho}\frac{\partial}{\partial\rho}\rho\frac{\partial}{\partial\rho}+\frac{1}{\rho^2}\frac{\partial^2}{\partial\phi^2}\right)\psi(\rho,\phi) + \left[U(\rho,\phi)+\lambda g_4\sum_{i<j}^{3}\delta(\alpha\rho|\sin(\phi-\phi_{ij})|)\right]\psi(\rho,\phi)=E_{EAA}\psi(\rho,\phi) \tag{99}$$

Finally, we describe $\psi(\rho,\phi)$ as a sum over adiabatic channel function:

$$\psi(\rho,\phi)=\sum_{n=0}^{\infty}\rho^{-1/2}f_n(\rho)\chi(\rho;\phi) \tag{100}$$

where $\chi(\rho;\phi)$ satisfy the fixed-ρ equation:

$$-\frac{1}{2\mu_4\rho^2}\frac{\partial^2\chi_n}{\partial\phi^2}+U(\rho,\phi)\chi_n+\lambda g_4\sum_{i<j}^{3}\delta(\alpha\rho|\sin(\phi-\phi_{ij})|)\chi_n=U_n(\rho)\chi_n \tag{101}$$

As it's name suggests, the fixed-ρ equation fixes ρ, and the system is solved over the remaining coordinate ϕ. This is shown graphically in figure (8).

5.3 The 4-Body λ Boundary Condition

In order to incorporate arbitrary heavy-heavy couplings (or λ), one must enforce a delta function boundary condition at $\phi=\pi/6$. This is done using the method outlined in section (3) and is very similar to the λ boundary condition in section (4). We begin by rearranging Eq. (101)

$$\frac{\partial^2\chi_n}{\partial\phi^2}=2\mu_4 g_4\rho^2\lambda\sum_{i<j}^{3}\delta(\alpha\rho|\sin(\phi-\phi_{ij})|)\chi_n+2\mu_4\rho^2[U(\rho,\phi)-U_n(\rho)]\chi_n \tag{102}$$

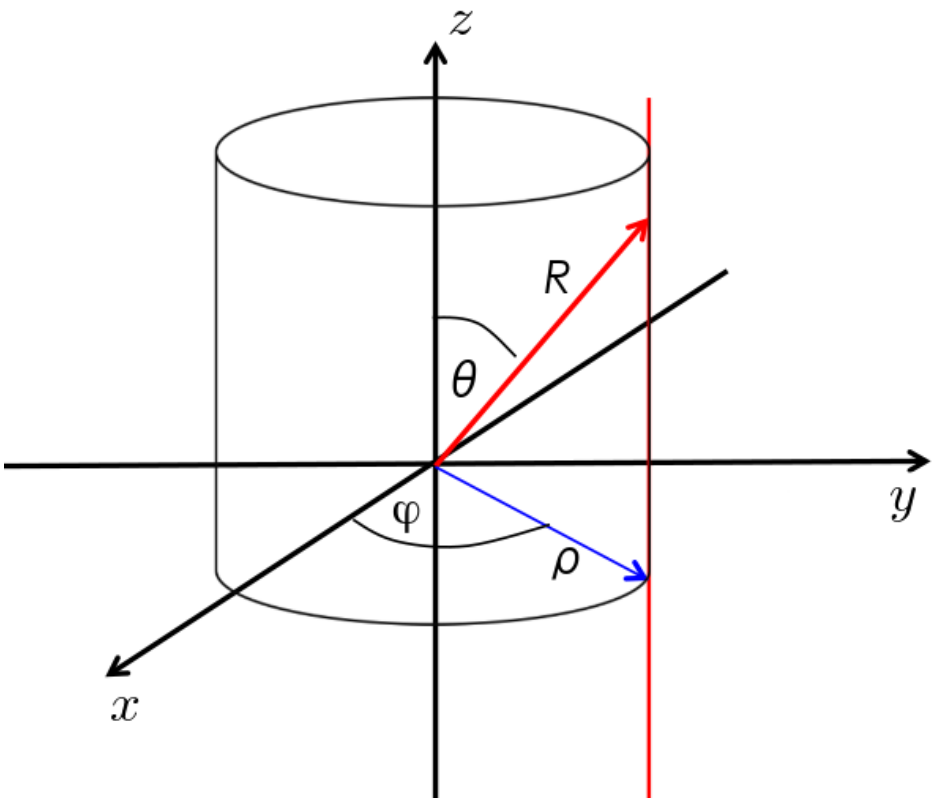

Figure 8: The coordinate space in both Cartesian and spherical-polar. It is easy to see that when ρ is fixed, the resulting red line is where Eq. (101) is solved on. Figure adapted from [15] with permission.

We then integrate both sides across an interval 2ϵ about $\pi/6$ we have:

$$\left.\frac{\partial\chi_n}{\partial\phi}\right|_{\pi/6+\epsilon} - \left.\frac{\partial\chi_n}{\partial\phi}\right|_{\pi/6-\epsilon} = \frac{2\mu_4 g_4\rho^2\lambda}{|\alpha\rho|}\int_{\pi/6-\epsilon}^{\pi/6+\epsilon}\sum_{i<j}^{3}\frac{\delta(\sin(\phi-\phi_{ij}))}{|\operatorname{sgn}(\phi-\phi_{ij})|}\chi_n + 2\mu_4\rho^2\int_{\pi/6-\epsilon}^{\pi/6+\epsilon}[U(\rho,\phi)-U_n(\rho)]\chi_n \quad (103)$$

Since $\left.\frac{\partial\chi_n}{\partial\phi}\right|_{\pi/6-\epsilon} = -\left.\frac{\partial\chi_n}{\partial\phi}\right|_{\pi/6+\epsilon}$, we have:

$$\left.\frac{\partial\chi_n}{\partial\phi}\right|_{\pi/6+\epsilon} = \frac{\mu_4 g_4\rho\lambda}{\alpha}\int_{\pi/6-\epsilon}^{\pi/6+\epsilon}\delta(\phi-\pi/6)\chi_n\partial\phi + \mu_4\rho^2\int_{\pi/6-\epsilon}^{\pi/6+\epsilon}[U(\rho,\phi)-U_n(\rho)]\chi_n \quad (104)$$

As before we then take the limit as $\epsilon \to 0$:

$$\frac{1}{\chi_n}\left.\frac{\partial\chi_n}{\partial\phi}\right|_{\pi/6} = \frac{\mu_4 g_4\rho\lambda}{\alpha} + \mu_4\rho^2\int_{\pi/6-\epsilon}^{\pi/6+\epsilon}[U(\rho,\phi)-U_n(\rho)]\chi_n \to 0 \quad (105)$$

Plugging in expressions for μ_4, g_4, and α, we're left with:

$$\frac{1}{\chi_n}\left.\frac{\partial\chi_n}{\partial\phi}\right|_{\pi/6} = \frac{\rho\lambda(1+\beta)}{\sqrt{2}\beta}\left(\frac{\beta}{3+\beta}\right)^{1/6} \quad (106)$$

Eq. (106) is a correction to the formula presented in [16]. This correction is due to the correction in Eq. (84).

The 4-body boundary conditions presented for different parity and interactions are summarized in table (2). For an in depth discussion of these boundary conditions, see ref. [16]. The boundary condition in Eq. (106) is for positive parity bosons at $\phi = \pi/6$, as the boundary condition at $\phi = 0$ does not change when the interaction strength of the heavy particles changes. Note how Eq. (106) satisfies both boson boundary conditions (non-interacting and infinitely repulsive) for $\lambda = 0$ (non-interacting) and $\lambda = \infty$ (infinitely repulsive). Also note that the boundary conditions for infinitely repulsive bosons and fermions are the same. Thus we expect as the interaction is increased by increasing λ, the 4-body spectrum and atom-trimer scattering length should vary smoothly to the infinitely repulsive fermionic solution. This mapping of solutions can be seen in the HHHL phase diagram in the following section.

5.4 4-Body Phase Diagram

Figures 9(a), 9(c), and 9(e) show the hyperradial potential curves $U_n(\rho)$ obtained by solving the fixed-ρ Eq. (101) using the potential energy surface. At large ρ, the lowest potential curves converge to the appropriate

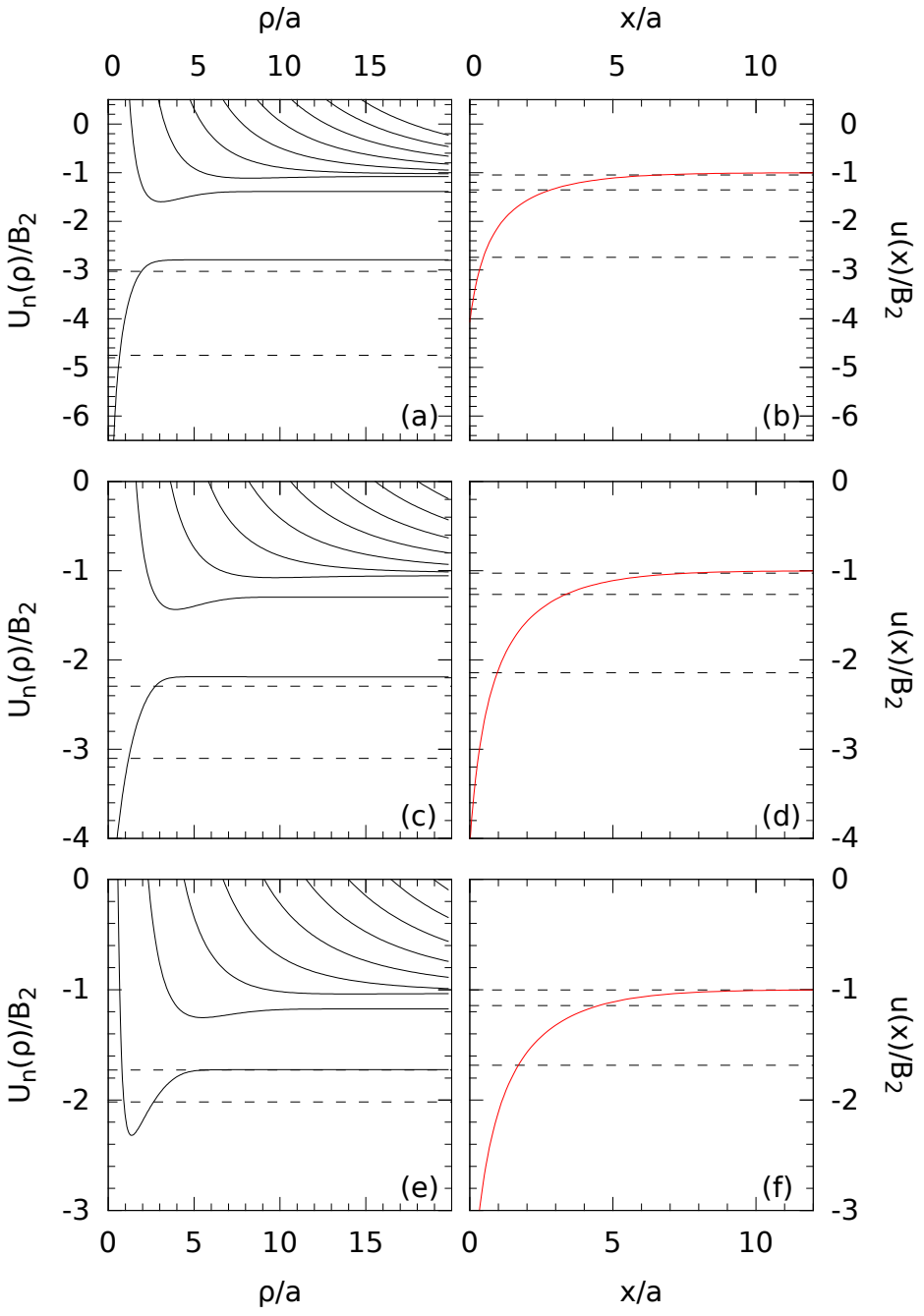

Figure 9: Graph (a) shows the bosonic hyperradial potential curves describing the heavy-particle dynamics in the HHHL system ($\lambda = 0$), while graph (b) shows the corresponding Born-Oppenheimer potential curve for the HHL system. Graphs (c) and (d) show similar curves except for a intermediate bosonic case ($\lambda = 0.3$). Graphs (e) and (f) show similar curves except for fermions ($\lambda = \infty$) All graphs are for $\beta^{-1} = 22.08$.

$\phi = 0$	Positive Parity (+)	Negative Parity (-)
Bosons	$\left.\frac{d\chi}{d\phi}\right\|_0 = 0$	$\chi\|_0 = 0$
Fermions	$\chi\|_0 = 0$	$\left.\frac{d\chi}{d\phi}\right\|_0 = 0$
$\phi = \pi/6$	Non-Interacting	Infinitely Repulsive
Bosons	$\left.\frac{\partial\chi}{\partial\phi}\right\|_{\pi/6} = 0$	$\chi\|_{\pi/6} = 0$
Fermions	$\chi\|_{\pi/6} = 0$	$\chi\|_{\pi/6} = 0$

Table 2: Boundary conditions on χ

HHL bound-state energy. Figure 10 shows the spectrum and atom-trimer scattering lengths of the HHHL

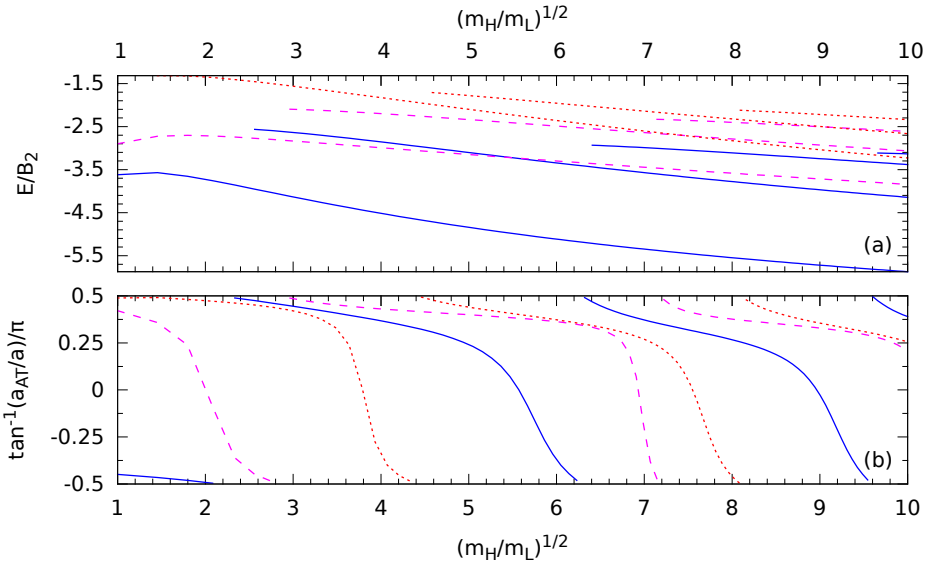

Figure 10: Graph (a) shows the energy spectrum for the four-body system as a function of $\beta^{-1/2}$. Graph (b) shows $\tan^{-1}(a_{AT}/a)/\pi$, where a_{AT} is the atom-trimer scattering length. Solid blue curves represent the noninteracting bosonic H particles ($\lambda = 0$). The dashed purple curves represent the interacting bosonic H particles ($\lambda = 10$). The dotted red curves represent the noninteracting fermionic particles or fermionized H particles with $\lambda = \infty$.

system with noninteracting positive-parity bosonic heavy atoms for 0, 0.3, and ∞ values of λ.

Figure 11 shows the HHHL phase diagram. The phase diagram is constructed in an analogous way as the HHL phase diagram. However, the dotted black line now represents where the three-body bound state energies of the HHH and HHL trimers are equal. The HHH energies were calculated from the work of ref. [14], and the HHL energies were simply the values found in the three-body stage of the total calculation. The number of four-body bound states is indicated by n on the graph.

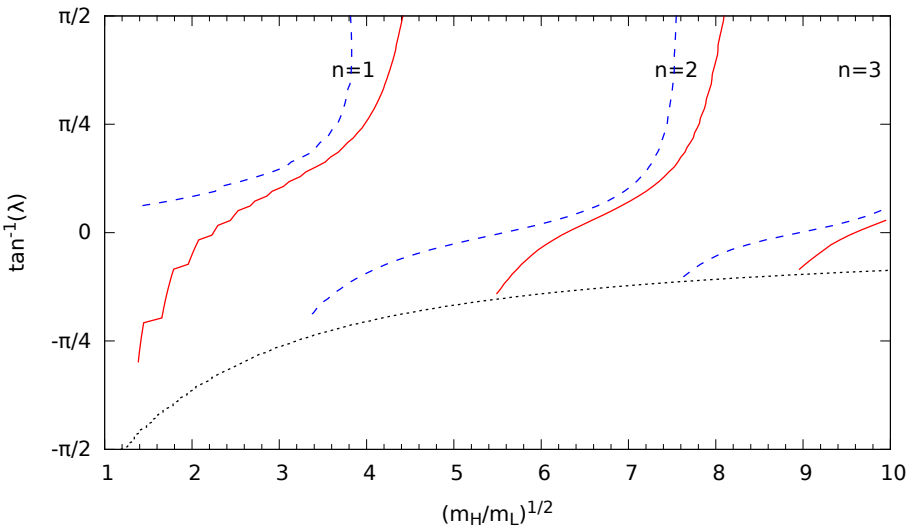

Figure 11: Phase diagram for the HHHL system as a function of $\beta^{-1/2}$ and $\arctan(\lambda)$. The dash-dotted blue line denotes the positions of the zeros (i.e. where the atom-trimer scattering length changes sign). The solid red curves denote the positions of the asymptotes (i.e. where the system begins to support a new bound-state). The dotted black line represents where the HHH and HHL three-body energies are equal.

6 Boundary Conditions with B-Splines

The boundary condition shown in Eqns. (59) and (106) are enforced using B-splines. B-splines, or basis splines, are a subset of splines, which are piecewise polynomial functions with a high degree of smoothness where the piecewise sections intersect. These intersections are known as knots. A spline can be expressed as a linear combination of B-splines. A typical set of B-splines are shown in figure (12). Note the low support of the individual B-splines. This means that each B-spline is non-zero for only a small range. Thus, only a few B-splines overlap at any given position. For this thesis, $\psi(x)$ and $\chi(\phi)$ are both expanded in a basis

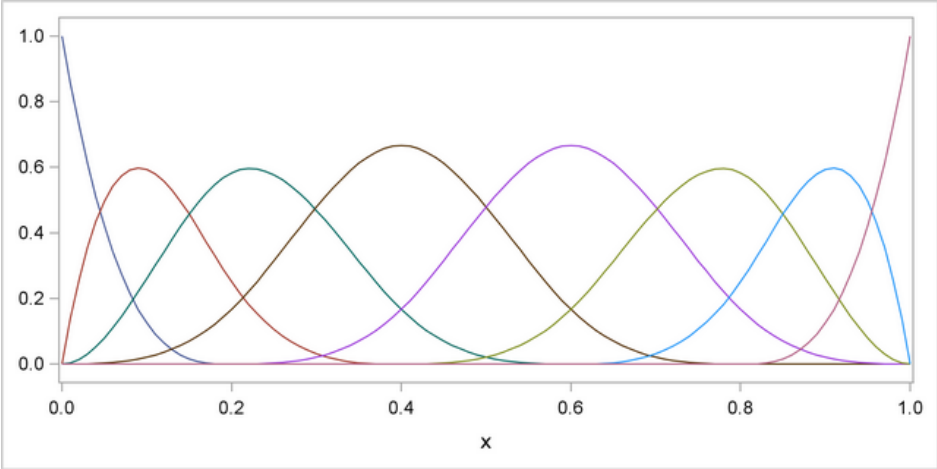

Figure 12: Typical B-splines used in this thesis and [16].

of B-splines. The following section will explicitly show how to enforce a derivative discontinuity in $\psi(x)$ at $x = 0$. The same process is used to enforce the derivative discontinuity on $\chi(\phi)$ at $\phi = \pi/6$.

$$\psi(x) = \sum_n C_n B_n(x) \tag{107}$$

Along the boundaries, there are only two non-zero B-splines:

$$\psi(x)|_{x=0} = \widetilde{B} = C_1 B_2 + C_2 B_2 \tag{108}$$

Here only the left boundary is considered, since that is where the derivative discontinuity is enforced. It is worthwhile to consider some of the properties of these two B-splines. For this thesis and [16], these B-splines were chosen such that B_1 has the equal and opposite slope of B_2. This makes the boundary conditions considered in [16] very easy to enforce. To enforce a zero-value boundary condition, one simply sets $C_1 = 0$ and $C_2 = 1$, since B_2 has a value of 0 at $x = 0$. In order to enforce a zero-derivative boundary condition one simply sets $C_1 = C_2 = 1$. This ensures that the slope at $x = 0$ is 0. In order to consider arbitrary λ Eq. (108) is substituted into Eq. (59).

$$\left.\frac{\psi'}{\psi}\right|_{\epsilon\to 0} = \frac{C_1 B_1'(0) + C_2 B_2'(0)}{C_1 B_1(0) + C_2 B_2(0)} = K \tag{109}$$

Here K is the right-hand-side of Eq. (59). One then solves Eq. (109) for C_2/C_1.

$$\frac{C_2}{C_1} = \frac{B_1(0) - K B_1'(0)}{B_2(0) - K B_2'(0)} \tag{110}$$

$B_1(0)$ and $B_2(0)$ and their derivatives are calculated using routines from [2]. Eq. (110) ensures that $\psi(x)$ satisfies the derivative discontinuity specified by Eq. (59). By examining equations (110) and (59) it is clear that this general boundary condition satisfies the previous edge-cases considered in [16]. This also applies to the HHHL system, where one considers Eq. (106) rather than Eq. (59).

7 Conclusion

The three-body and four-body spectra, atom-dimer, and atom-trimer scattering lengths were calculated for the HHL and HHHL systems for arbitrary values of lambda. The heavy particles were considered to be positive parity bosons with arbitrary interaction strengths throughout. In the HHL system, the Born-Oppenheimer method has good agreement with the results of [8]. An HHL phase diagram shares the same

qualitative features as the phase diagram presented by [8] who used analytical methods. A similar HHHL phase diagram was found. As in the HHL system, it was found that the the spectrum and atom-trimer scattering length varied smoothly as $\lambda \to \infty$. Thus the extension of arbitrary HH particle interaction in Mehta's [16] work has been realized.

This work was done in the "3+1" branch of the few-component problem. It is possible that similar methods could be used to approach systems in other branches, such as the "2+2" (HHLL) system. Further work could also be done to increase the accuracy of these results, by calculating the diagonal correction for the HHHL system.

8 Acknowledgements

I would like to thank Nirav Mehta for his guidance and support on this thesis. I would also like to thank Liam Fox for his contributions and discussions during this work. Finally, I would like to thank Trinity University for providing the funding for this work.

References

[1] T. Bergeman, M. G. Moore, and M. Olshanii. In: *Phys. Rev. Lett.* 91 (2003), p. 163201.

[2] C. de Boor. *A Practical Guide to Splines*. Springer, 2001. ISBN: 9780387953663.

[3] M. Born and J. R. Oppenheimer. In: *Annalen der Physik* 389 (1927), p. 20.

[4] L. Dodd. In: *J. Math. Phys.* 11 (1970), p. 207.

[5] A. Görlitz et al. In: *Phys. Rev. Lett.* 87 (2001), p. 130402.

[6] M. Greiner et al. In: *Phys. Rev. Lett.* 87 (2001), p. 160405.

[7] David Jeffrey Griffiths and Edward G Harris. *Introduction to quantum mechanics*. Vol. 2. Prentice Hall New Jersey, 1995.

[8] O. I. Kartavtsev, A. V. Malykh, and S. A. Sofianos. In: *Zh. Eksp. Teor. Fiz.* 135 (2009), p. 419.

[9] T. Kinoshita, T. Wenger, and D. S. Weiss. In: *Science* 305 (2004), p. 1125.

[10] T. Kinoshita, T. Wenger, and D. S. Weiss. In: *Nature (London)* 440 (2006), p. 900.

[11] A. E. Leanhardt et al. In: *Phys. Rev. Lett.* 89 (2001), p. 040401.

[12] G.P. Lepage. In: (1997). DOI: `arXiv:nucl-th/9706029`.

[13] E. Lieb and W. Liniger. In: *Phys. Rev.* 130 (1963), p. 1605.

[14] J. B. McGuire. In: *J. Math. Phys.* 5 (1964), p. 622.

[15] N. P. Mehta. 2014. URL: http://meetings.aps.org/link/BAPS.2014.DAMOP.U3.7.

[16] N. P. Mehta. In: *Phys. Rev. A* 89 (2014), p. 052706.

[17] S. Murmann et al. In: *Phys. Rev. Lett.* 114 (2015), p. 080402.

[18] M. Olshanii. In: *Phys. Rev. Lett.* 81 (1998), p. 938.

[19] A. Reinhard et al. In: *Phys. Rev. Lett.* 110 (2013), p. 033001.

[20] Y. Suzuki and K. Varga. *Stochastic Variational Approach to Quantum-Mechanical Few-Body Problems*. Springer Science & Business Media, 1998. ISBN: 3540651527.

[21] H. B. Thacker. In: *Phys. Rev. D* 11 (1974), p. 838.

[22] B. Laburthe Tolra et al. In: *Phys. Rev. Lett.* 92 (2004), p. 190401.

[23] C. Yang and C. Yang. In: *J. Math. Phys.* 10 (1969), p. 1115.

[24] C. N. Yang. In: *Phys. Rev. Lett.* 19 (1967), p. 1312.